ACS ES&T Water

pubs.acs.org/estwater

Article

Solvent-Free Process to High-Flux Ultrafiltration Membranes: Spray Coating of Water-Dispersed Carbon Nanotubes

Dongwei Ma, Xiangyue Ye, Xiansong Shi, Jiemei Zhou, and Yong Wang*

Cite This: ACS EST Water 2022, 2, 895−903

Read Online

ACCESS | Metrics & More | Article Recommendations | Supporting Information

ABSTRACT: Mainstream ultrafiltration (UF) membranes are typically produced from the phase inversion of polymer solutions and suffer from the extensive use of organic solvents and disposal of organic wastewater. Therefore, it remains highly demanding for clean processes to produce UF membranes at no expense of separation performances. Herein, we report the preparation of high-performance carbon nanotube (CNT)-based membranes without using any organic solvents. CNTs are first homogeneously dispersed in water with the assistance of an amphiphilic block copolymer. The CNT-based membranes, composed by a separation layer of stabilized CNT networks and macroporous supports, are obtained by spray coating aqueous CNT dispersions. The pore sizes of thus-prepared CNT UF membranes are easily tuned by controlling the diameter of CNTs or the spraying volumes of the CNT dispersions. The CNT membranes exhibit superior water permeance (460−7750 L m^{-2} h^{-1} bar^{-1}) compared with membranes produced by other methods with similar pore sizes. This solvent-free process enabled by spray coating is expected to extend to other water-dispersible low-dimensional building blocks in clean preparation of various high-performance membranes.

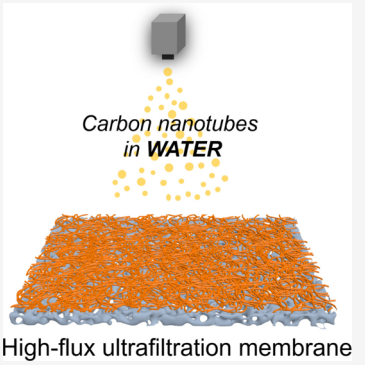

KEYWORDS: *ultrafiltration, carbon nanotube, spray coating, block copolymer, water purification*

1. INTRODUCTION

Ultrafiltration (UF) membranes are of especial interest for removing colloidal contaminants during the production of drinking water and wastewater treatment.[1] Commercial UF membranes are mostly prepared by nonsolvent induced phase separation (NIPS), which involves polymer solutions in organic solvents and precipitation in nonsolvent (generally water) coagulation bath to generate a porous asymmetric structure.[2] Over the past few decades, NIPS-based membranes have been utilized in nearly every corner of membrane-based separation fields. However, NIPS-based membranes suffer from the use of toxic aprotic solvents, which are harmful for the environment and destined to be banned.[3] Recently, the European Union restricted the use of *N*-methyl-2-pyrrolidone (NMP) after May 2020.[4] Besides, the water bath will generate around 50 billion liters of organic wastewater each year.[5] Hence, manufacturing processes of high-performance UF membranes without the use of toxic solvents are urgently demanded.[6,7]

Replacing toxic solvents, such as NMP, *N*,*N*-dimethylformamide (DMF), and *N*,*N*-dimethylacetamide (DMAc), with greener solvents is a direct solution to this sticky issue.[8] Dong et al. fabricated polysulfone (PSf) UF membranes using eco-friendly solvents (Rhodiasolv PolarClean and γ-valerolactone).[9] Except the benefit of sustainability, the cost of the alternative nontoxic solvents and the performances of membranes prepared from greener solvents need to be optimized further. Li et al. reported a simple and modified approach of freeze-drying to prepare poly(vinylidene fluoride) (PVDF) UF membranes by combining crystallization and diffusion (CCD).mem[10,11] In the CCD method, a relative greener solvent, dimethyl sulfoxide (DMSO), was used and asymmetric PVDF membranes with the pore size down to 15 nm were successfully produced. However, the cooling temperature of the polymer solidification is very low (−30 °C) and the leakage of organic DMSO in the ice water bath should be in consideration. A solution to completely eliminate the disposal of organic wastewater needs radical innovation to NIPS or using water as solvent/nonsolvent during phase inversion. Polyelectrolytes (PE), as a class of polymers, could be used to prepare reverse osmosis,[12] nanofiltration,[13] and ultrafiltration membranes without usage of organic solvents because of their water solubility. Recently, Sadman et al.[14] utilized polyelectrolyte complex (PEC) to prepare UF membranes without the use of organic solvents. The resultant PEC membranes were able to reject 100 nm size polystyrene beads with a water permeance in the range 95−375 L m^{-2} h^{-1} bar^{-1}. Similarly, de Vos and his team explored a fascinating, sustainable, and environmentally friendly aqueous phase

Received: March 14, 2022
Revised: April 12, 2022
Accepted: April 24, 2022
Published: May 4, 2022

https://doi.org/10.1021/acsestwater.2c00125
ACS EST Water 2022, 2, 895−903

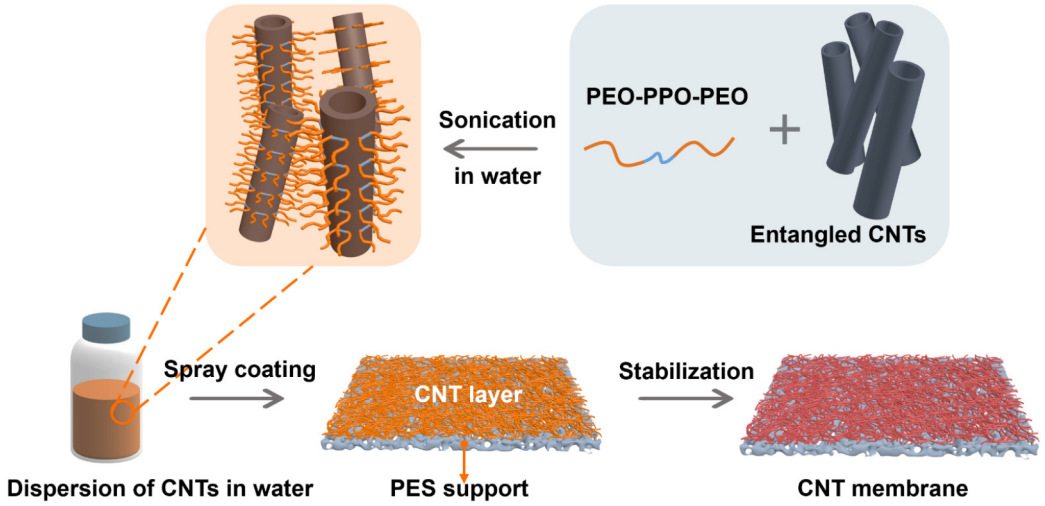

Figure 1. Schematic diagram for the preparation of CNT membranes.

separation (APS) method to prepare PEC-based UF membranes by utilizing water as a solvent at a low or high pH and a nonsolvent at the opposite pH. However, the highest permeability of the resulted UF membranes is below 25 L m^{-2} h^{-1} bar^{-1} with a BSA retention of 85%.[15]

Fibrous membranes composed of 1D nanomaterials (inorganic nanowires, polymeric nanofibers, and carbon nanotubes) are recognized as a solution to prepare high-flux UF membranes owing to their high porosity and interconnected interstices. Yu's group[16,17] obtained carbonaceous nanofiber membranes with a high permeance of 12000 L m^{-2} h^{-1} bar^{-1} and could reject gold nanoparticles completely. We are aware of that there were some reports on depositing carbon nanotubes (CNTs) on porous substrates to prepare composite UF membranes. For instance, Brady-Estévez et al.[18] vacuum-filtrated CNTs suspended in dimethyl sulfoxide to obtain a CNT filter with a permeance of 13 800 L m^{-2} h^{-1} bar^{-1}. Others[18,19] and our group[20] reported CNT UF membranes, which can remove bacteria and viruses absolutely and keep a high permeability. However, in these previous works, CNTs had to be dispersed in organic solvents, implying that the manufacturing processes remained solvent extensive. Jin and colleagues[21−24] dispersed single-walled CNTs in water under the assistance of sodium dodecyl benzenesulfonate. Then, they vacuum-filtrated or brush-painted CNT dispersions on macroporous support to obtain CNT membranes with remarkable fluxes. Zhou et al.[25] spray-coated CNTs on the polyether sulfone (PES) supports and obtained membranes with a high water permeance of 17 000 L m^{-2} h^{-1} bar^{-1}. All these results above manifested the great potential of fibrous membranes in UF. Here in this work, CNTs were applied to prepare high-flux UF membranes by taking advantage of the high porosity of 1D CNT networks, excellent mechanical strength, thermal stability, and tunable tube diameters. CNTs were homogeneously dispersed in water with the assistance of amphiphilic block copolymer of Pluronic F127, thus eliminating the use of toxic solvents on one hand, and spray coating of aqueous CNT dispersions onto porous substrates avoids the generation of organic wastewater during the formation of composite membranes with the assembled CNT networks as the separation layer on the other (Figure 1). The CNT networks were then stabilized by cross-linking the poly(ethylene oxide) (PEO) chains in F127 with glutaraldehyde. Thus-prepared CNT membranes possessed pores with diameters in the range 18−47 nm and exhibited high water permeances of 460−7750 L m^{-2} h^{-1} bar^{-1} depending on the diameter of CNTs. Our spray-processed CNT-based UF membranes are prepared from a more environment-friendly process requiring no organic solvents and are distinguished for their high flux of water compared to other membranes.

2. MATERIALS AND METHODS

2.1. Materials. Three types of multiwalled CNTs were provided from XFNANO Materials Technology Co., Ltd. The diameter and length of CNTs provided by the supplier are presented in Table 1. Block copolymer of Pluronic F127 (M_w= 12.6 kDa) was obtained from Sigma-Aldrich. Glutaraldehyde (GA, 50 wt % aqueous solution) was provided from Shanghai Macklin Biochemical Co. Ltd. Potassium hydroxide (KOH) was provided by Shanghai Aladdin Biochemical Technology Co. Ltd. Bovine serum albumin (BSA, 98%, 66 kDa) and phosphate buffered saline (PBS) tablets were purchased from MP Biomedicals, LLC. One piece of phosphate tablet was dissolved in 100 mL of pure water to obtain the buffer solution of BSA at a pH of 7.4, and the BSA concentration was 0.5 g L^{-1}. The aqueous colloid of monodispersed gold nanoparticles with a particle size of 50 nm (50 nm Au NPs) were purchased from British Biocell International (BBI). The PES microfiltration membranes with a nominal pore size of ca. 0.45 μm were purchased from Haiyan Xindongfang Plastic Technology Co., Ltd. and used as the supports to obtain CNT-based composite membranes. Pure water (conductivity: <5 μS cm^{-1}) was homemade and used in all experiments.

Table 1. Tube Diameter and Length of CNTs Provided by the Supplier

CNT codes	outer diameter (nm)	length (μm)	purity (%)
CNT-1	10−20	10−30	>98
CNT-2	8−15	~50	>98
CNT-3	4−6	10−20	>98

2.2. Preparation of CNT Dispersions. CNTs (0.5 mg mL^{-1}) were sonicated by a probe ultrasonicator (probe diameter is 10 mm) at the power of 650 W for 60 min. To

https://doi.org/10.1021/acsestwater.2c00125
ACS EST Water 2022, 2, 895−903

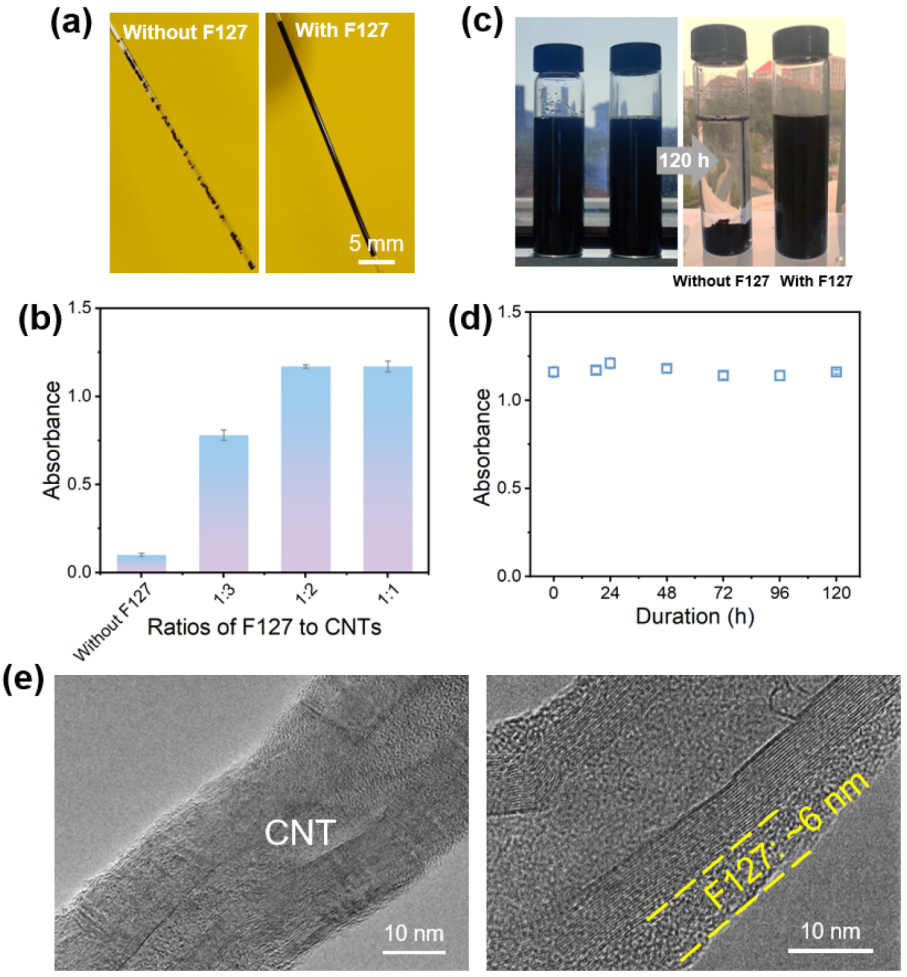

Figure 2. Dipersity and long-term stability of CNT-1 aqueous dispersions. (a) CNT-1 dispersions sucked in capillaries to present the dispersity of CNTs in water. (b) Absorbance intensity of CNT-1 dispersions detected by UV−visible spectrometry. (c) CNT-1 dispersions without F127 and with 1:2 F127/CNT preserved for 120 h at room temperature. (d) Stability of CNT-1 dispersions at a ratio of F127/CNTs = 1:2. (e) Transmission electron microscopy (TEM) micrographs of CNT-1 and F127 coated CNT-1.

disperse CNTs well, F127 (0.25 mg mL^{-1} for CNT-1 and CNT-2 dispersions, and 0.5 mg mL^{-1} for CNT-3 dispersions) was mixed with the CNT suspensions and stabilized CNTs for another 30 min at power of 100 W. All sonication processes were performed in a ice bath. As-prepared nascent CNT dispersions were centrifuged (3000 rpm, 5 min for CNT-1 and CNT-2 dispersions, and 10 000 rpm, 5 min for CNT-3 dispersions) to remove any undispersed CNTs. Well-dispersed CNT supernatant was suctioned and collected for use.

2.3. Preparation of CNT Membranes. The spraying conditions and setup of the spray machine were set according to our latest work.[26] Generally, PES support with a size of 15 × 10 cm^2 was flattened on the horizontal heating plate. Afterward, the well-dispersed CNT dispersions were ejected and atomized onto the PES support by the nozzle. The nozzle was moved repeatedly to form a uniform and defect-free CNT layer with the stack of the CNT networks. Afterward, F127 in CNT membranes were cross-linked by GA.[27] CNT membranes were immersed in GA aqueous solution, and a certain amount of KOH was mixed into the solution as the catalyst for the cross-linking reaction. The CNT membrane/GA/KOH mixture was reacted at 95 °C for 72 h. As presented in Figure S1, the disappearance of strong characteristic absorption peaks of −OH groups at ∼3410 cm in the cross-linked CNT membranes indicated the successful cross-linking between F127 in CNT membranes and GA.

2.4. Characterization. CNT dispersions were diluted 30 times by pure water to characterize the dispersity and stability of the CNT dispersions by a UV−visible spectrometer (Nanodrop 2000C, Thermo Fisher Scientific) at a specific absorbance of 260 nm. Scanning electron microscopy (SEM) micrographs were captured by a Hitachi S4800 at an operating voltage of 5 kV and a current of 10 μA. The cross sections of the sample were obtained by immersing the CNT-based membranes in liquid nitrogen and rupturing quickly. The surfaces and cross sections of the sample were sputter-coated by gold to reduce electric discharge before observations. The values of membrane thickness were measured by the cross-sectional SEM micrographs. The surface visual average pore sizes and porosities were obtained from SEM images analyzed by the image software of ImageJ. The cross-linked CNT-based membranes were characterized by Fourier transform infrared (FTIR) spectrometry (Nicolet 8700, Thermo Fisher Scientific) using attenuated total reflectance (ATR) mode.

The average pore sizes of the CNT-based membranes were measured by a porometer (iPore-1500AEX-Clamp, Porous Material Inc.) according to gas−liquid displacement porosimetry. CNT membranes were put into the porometer and

https://doi.org/10.1021/acsestwater.2c00125
ACS EST Water 2022, 2, 895−903

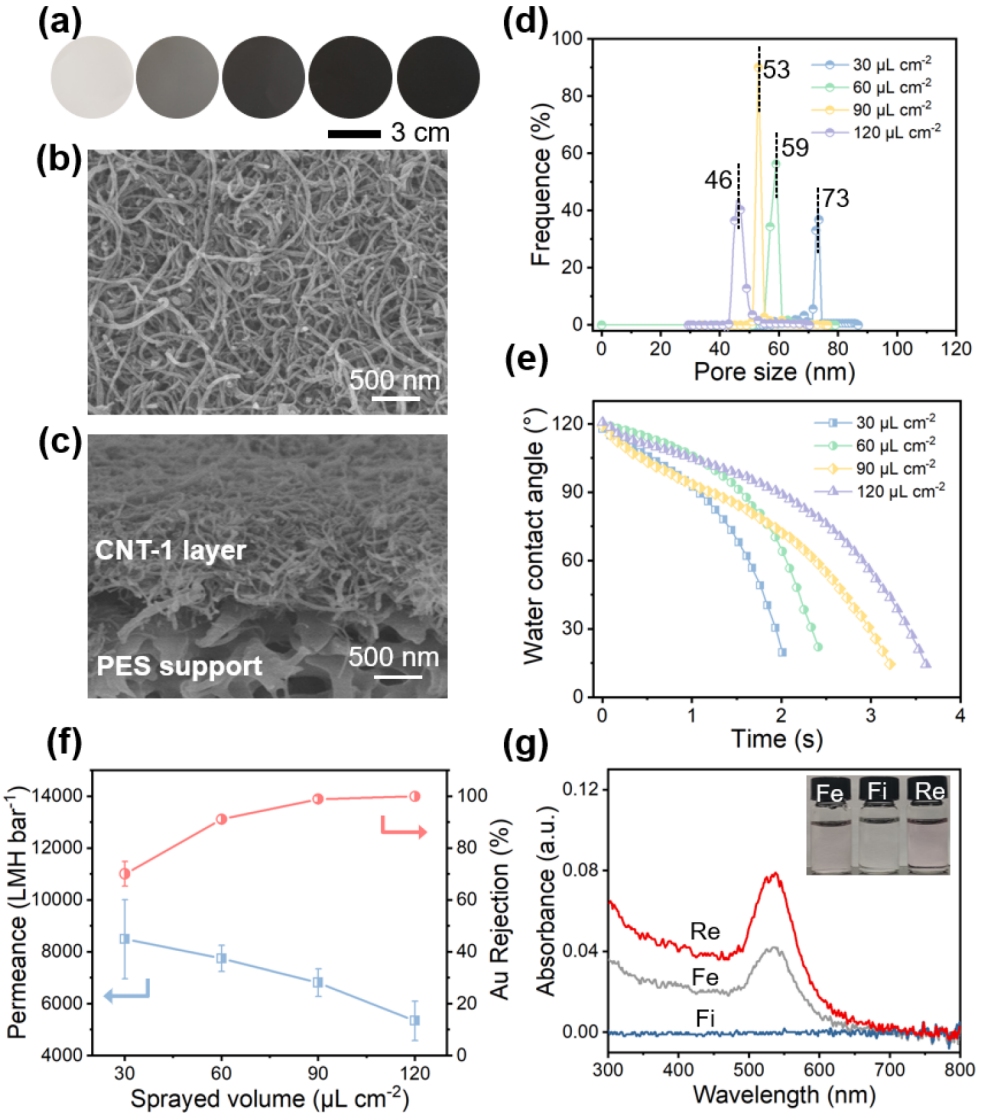

Figure 3. Characterizations and performances of CNT-1 membranes. (a) Digital photos of the CNT-1 membranes with variable sprayed volumes: 0, 30, 60, 90, and 120 μL cm^{-2}, respectively. (b and c) Surface and cross-sectional SEM micrographs of the CNT-1 membrane with a sprayed volume of 120 μL cm^{-2}. (d) Pore-size distributions of the CNT-1 membranes characterized by a porometer. (e) Dynamic water contact angle tests of the CNT-1 membranes. (f) Water permeances and 50 nm Au NPs rejections of the CNT-1 membranes prepared with different sprayed volumes. (g) UV−visible absorption spectra of feed (Fe), filtrate (Fi), and retentate (Re) of 50 nm Au NPs; inset in (g) is the digital photo of feed, filtrate, and retentate of 50 nm Au NPs.

wetted with a customed wetting liquid, Galwick, which was purchased from a supplier and had a surface tension of 15.9 mN m^{-1}. The Washburn equation was employed to calculate the membrane pore size as follows:

$$D = 4\gamma\cos\theta/p \quad (1)$$

where D is the diameter of the membrane pore; γ is the surface tension of the wetting liquid; θ is the contact angle of the wetting liquid on the membrane surface; and p is the operation gas pressure.

The water contact angles (WCAs) were performed by a contact angle goniometer (Dataphysics OCA25). Five microluters of DI water was dropped onto the membrane surface to get the value of static and dynamic contact angle, and images of the water droplets were captured by a high-speed video camera equipped on the goniometer. The reported values of WCAs were tested three times at least.

2.5. Filtration Test. Pure water permeances (PWPs) and rejections were tested utilizing a cross-flow apparatus under a pressure of 1 bar. The effective permeating membrane area was 7.1 cm^2. Membrane coupons were precompacted at a pressure of 1.5 bar for a steady water flux before the values of PWP were recorded at a pressure of 1 bar. The PWP was calculated by eq 2:

$$\mathrm{PWP} = V/(A \times t \times P) \quad (2)$$

where PWP (L m^{-2} h^{-1} bar^{-1}, LMH bar^{-1}) represents the pure water permeance of membrane, V (L) is the permeating volume of water, t (h) is the testing duration, and P (bar) is the transmembrane pressure. The separation ability of the CNT membrane was represented by the rejections to 50 nm Au NPs and BSA solutions. The 50 nm Au NPs and BSA concentrations in the feeds, permeations, and retentates were detected by a UV−visible feature absorption spectrometer at

https://doi.org/10.1021/acsestwater.2c00125
ACS EST Water 2022, 2, 895−903

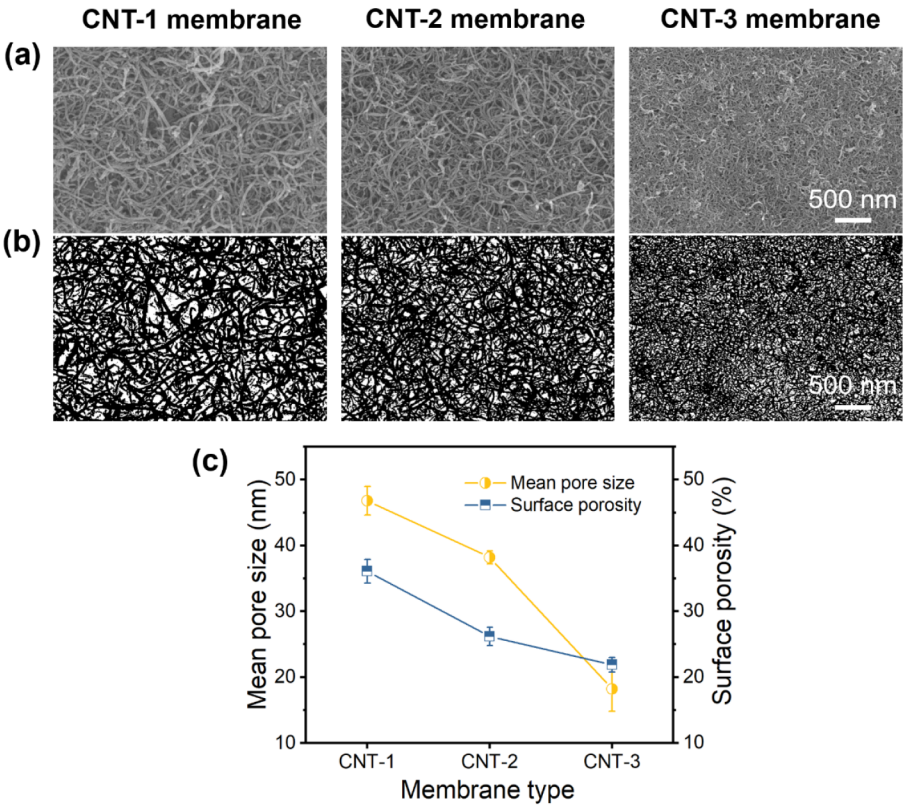

Figure 4. Pore-size distributions of CNT membranes. (a) SEM micrographs of CNT membranes spray-assembled by CNT-1, CNT-2, and CNT-3. (b) SEM micrographs of the CNT membranes processed by ImageJ software to present the average pore sizes and surface porosities of the CNT membranes; white parts represent pores and black parts are CNTs. (c) Mean pore sizes and surface porosities of CNT membranes.

~520 and ~280 nm, respectively. The rejection rates were calculated according to eq 3:

$$R = 100\% \times (1 - C_p/C_f) \quad (3)$$

where C_p and C_f (g L^{-1}) are 50 nm Au NPs or BSA concentrations in the permeations and the feeds, respectively.

3. RESULTS AND DISCUSSION

3.1. Dispersion of CNTs in Water. The triblock copolymer (PEO-*b*-PPO-*b*-PEO, F127) composed of poly(ethylene oxide) (PEO) and polypropylene oxide (PPO) was used to disperse CNTs (CNT-1, diameter of 10−20 nm, length of 10−30 μm) in water. The mass ratios of F127 to CNTs were systematically investigated to select an optimal condition for dispersing CNTs well. As shown in Figure 2a, CNTs were aggregated without the assistance of F127, indicating the poor dispersity of the CNT-1 aqueous suspension. In stark contrast, CNTs were dispersed well in water in the presence of F127. UV−visible spectrometry was used to quantitatively characterize the dispersity and stability of the CNT-1 dispersions with different ratios of F127 to CNTs. As shown in Figure 2b, the absorption strength of the CNT-1 dispersions had an improvement with the increased dosages of F127, indicating the improved dispersity of the CNT-1 dispersions. It was found that ratios lower than 1:2 did not produce sufficiently stable dispersion and were prone to jam the nozzle during spray coating. A ratio of 1:2 or higher produced good dispersions. That is, the critical point to obtain stable dispersions of CNTs is around 1:2. To minimize the dosage of F127, we chose to use a ratio of 1:2 in our following studies. CNT-1 dispersions maintained stable for 120 h with the aid of F127 (Figure 2c,d), which was necessary for the production of the CNT membranes during spraying. As shown in Figure 2e, a thin amorphous F127 layer with a thickness of ~6 nm tightly attached on the surface of the CNT-1 to improve the dispersity of CNTs. During the dispersion of CNTs, hydrophobic PPO blocks anchored at the surface of the CNT-1 via $\pi-\pi$ interactions,[28] and the hydrophilic PEO blocks solvated in water to repulse the aggregation between CNTs due to steric hindrance (Figure 1).

3.2. Spraying of CNT Dispersions to Prepare Composite Membranes. Aqueous CNT-1 dispersions were spray-coated on the surface of polyether sulfone (PES) supports to prepare CNT-1 membranes. As presented in Figure 3a, the pristine PES support appeared as a milky color, and the color of the membranes was changed from milky into a dark black after coated by the CNT-1 layers. As shown in Figure 3b,c and Figure S2a,b, the CNT-1 gradually covered the surface of the PES support and finally led to a thin CNT-1 layer with a tunable thickness in the range 280−1010 nm (Figure S2c) after increased sprayed volumes. The pore size of the CNT-1 membranes was also narrowed from 73 to 46 nm (Figure 3d) with the sprayed volume increase from 30 to 120 μL cm^{-2}. The narrowed pore size with the enlarged thickness of CNT-1 layer was highly consistent with the results reported.[24] The wetability of the CNT-1 membranes was analyzed by the results of water contact angles. As presented in Figure S2d, CNT-1 membranes with sprayed volumes of 30−120 μL cm^{-2} have a similar WCA value of ~120°. Meanwhile, the water droplets permeating speed was quick and the spreading time was around 2−4 s (Figure 2e). CNTs have a limited enhanced hydrophilicity, which might be due to the

https://doi.org/10.1021/acsestwater.2c00125
ACS EST Water 2022, 2, 895−903

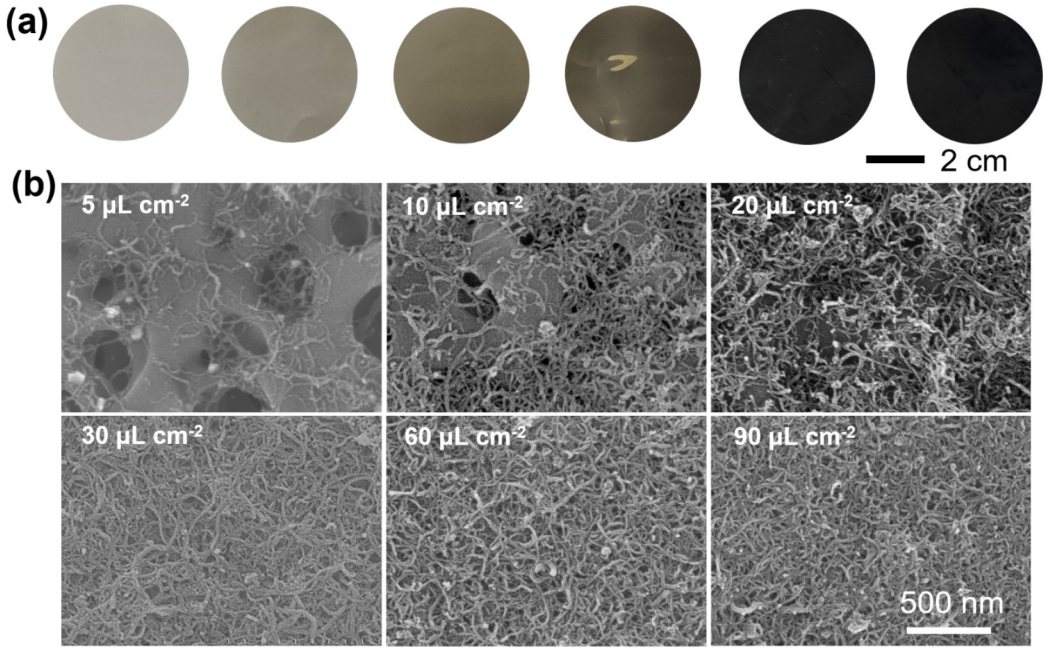

Figure 5. Surface mophlogies of CNT-1 membranes. (a) Digital images of the CNT-3 membranes with varied sprayed volumes: 5, 10, 20, 30, 60, and 90 μL cm^{-2}, respectively. (b) SEM micrographs of the CNT-3 membranes produced with varied sprayed volumes. All SEM micrographs in (b) have same maganification with a scale bar corresponding to 500 nm.

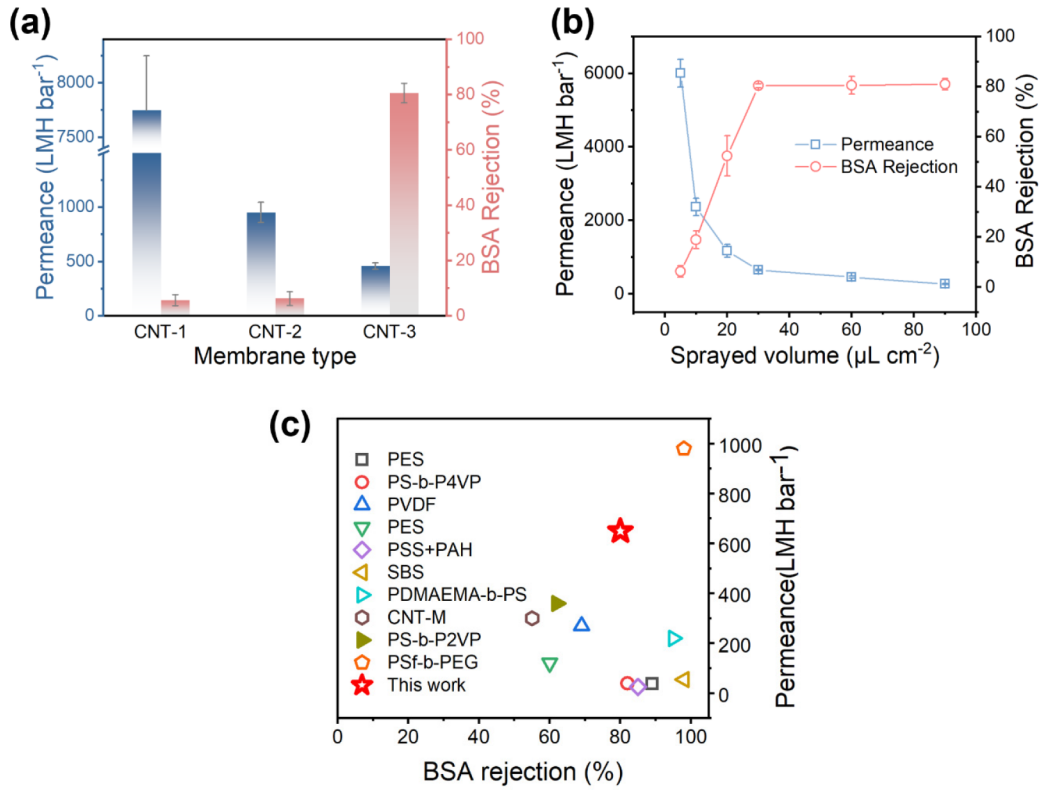

Figure 6. Performances of CNT membranes. (a) Performances of CNT membranes. (b) Performances of CNT-3 membranes. (c) Performance comparison of membranes.

not completely coated by F127 and the existence of bare CNTs on the membrane surface. For practical applications, good robustness and adhesive force between the selective layer and support of composite membranes are required. As shown in Figure S3, the CNT-1 membrane remained integrated without any cracks and pinholes after being repeatedly scratched by sandpaper for five cycles. Importantly, there was no noticeable difference in permeance and rejection of the membrane before and after abrasion resistance. We evaluated the long-stability of the CNT membranes as presented in Figure S4. The permeance of CNT membrane had a drop of 46.3% in the initial test of 3 h and finally stabilized at around

https://doi.org/10.1021/acsestwater.2c00125
ACS EST Water 2022, 2, 895−903

2100 L m^{-2} h^{-1} bar^{-1}, which was much higher than commercial UF membranes.

We investigated the influence of sprayed volumes on the separation performances of the CNT-1 membranes further. As shown in Figure 3f, CNT-1 membranes prepared with the sprayed volumes of 30−120 μL cm^{-2} exhibited water permeances in the range 8490−5430 L m^{-2} h^{-1} bar^{-1}, and their rejections to 50 nm Au NPs were increased from ∼70 to 100%. These results were due to the increased thicknesses and narrowed pore sizes of the CNT-1 selective layers. As presented in Figure 3g, the higher absorbance of Au NPs in the retentate and the deeper purple of the retentate indicates that the Au NPs are mainly rejected through the size exclusion not adsorption. These results demonstrate that the pore sizes, thicknesses, and performances of the CNT-1 membranes were highly adjustable by controlling the sprayed volumes of the CNT-1 dispersions during spray coating.

3.3. Effects of CNT Diameters on Membrane Morphologies and Pore Sizes. The pore sizes of the CNT networks are closely associated with the diameter of CNTs.[29] Herein, as presented in Table 1, CNTs with another two different diameters (CNT-2, diameter of 8−15 nm; and CNT-3, diameter of 4−6 nm) were chosen to produce CNT membranes with tunable pore sizes. We spray-coated CNT dispersions with a sprayed volume of 60 μL cm^{-2} on the surface of PES supports to obtain the CNT membranes. As shown in Figure 4a, the surface of the CNT membranes had a similar fiber-stacked nanostructure and the interstices between CNTs became narrowed with the decreased diameter of CNTs. As shown in Figure 4b, ImageJ was used to roughly present the surface visual average pore sizes and porosities of CNT membranes. Both the average pore sizes and the surface porosities of the CNT membranes decreased with the reduction of the tube diameter (Figure 4c). CNT membranes with mean pore sizes of 18−47 nm were stacked by the CNTs with the diameter scattering in the range 4−20 nm.

We systematically investigated the impact of sprayed volume on the morphology of the CNT-3 membranes further. As presented in Figure 5a, the surface color of CNT-3 membranes gradually darken from gray to black with the increased sprayed volumes from 5 to 90 μL cm^{-2}. As shown in the SEM images of CNT-3 membranes prepared with sprayed volumes of 5 to 90 μL cm^{-2} (Figure 5b), increased sprayed volumes led to more densely packed CNT-3 networks, and the overall networks still remained a highly porous structure. In the spray-coating process, CNT-3 gradually covered the macropores of the PES supports with increased sprayed volumes and eventually produced thin and defect-free CNT-3 selective layers.

3.4. Effects of CNT Diameters on Membrane Performances. As shown in Figure 6a, the pure water permeances of CNT membranes were dramatically dropped and a large improvement of BSA rejections showed with the reduction of CNT diameter. CNT-1 membranes had a superior water permeance of ∼7700 L m^{-2} h^{-1} bar^{-1} and a negligible rejection of 6% to BSA. CNT-2 membranes had a moderate water permeance of 950 L m^{-2} h^{-1} bar^{-1} and 6.3% BSA rejection. CNT-3 membranes had a water permeance of 460 L m^{-2} h^{-1} bar^{-1} and a much higher BSA rejection of 80%. These results of BSA rejections demonstrate that the pore sizes of the CNT membranes are effectively narrowed by tailoring the diameter of CNTs, which is highly consistent with the results of SEM characterizations. The higher permeance of the CNT-1 membrane is a result of higher porosity and larger pore size of the CNT-1 selective layer, which was highly consistent with the reported carbonaceous nanofiber membranes.[16,17] The relatively high BSA rejections of the CNT-3 membranes originate from the narrowed interstices between nanotubes.

Besides, we systematically investigated the impact of sprayed volume on permeance and BSA rejection of the CNT-3 membrane. As shown in Figure 6b, the permeances of the CNT-3 membranes decreased from ∼6000 to 1170 L m^{-2} h^{-1} bar^{-1} while the sprayed volumes increased from 5 to 20 μL cm^{-2}. At the same time, the rejections to BSA increased from 6.3 to 52.4%. As the sprayed volumes increased to 30−90 μL cm^{-2}, the BSA rejections increased to ∼80% significantly. Besides, the water permeances were dropped to 650−270 L m^{-2} h^{-1} bar^{-1} due to the thickness increaments of the CNT-3 layers. As shown in Figure 6c and Table S1, compared with the performances of state-of-the-art membranes with similar pore sizes and produced by other methods, the spray-assembled CNT membranes have superior water permeances.

One may be concerned that the CNT membranes still use PES microfiltration membranes, which are typically prepared by the solvent-extensive NIPS process, as the supports. Actually, this issue can be solved by replacing the PES supports with "green" ones, for example, nonwoven fabrics that are prepared by the solvent-free process of melt blown spinning. Furthermore, it is also technically possible to use the spray-assembled CNT membranes alone as self-supporting membranes as CNTs have strong mechnical strength and no substrates are required.

4. CONCLUSIONS

In summary, we have demonstrated a solvent-free process to produce high-flux UF membranes enabled by spray coating of water-dispersed CNTs. The homogeneous and stable CNT aqueous dispersions can be obtained under the assistance of F127. The effective pore sizes of the CNT-based membranes are facilely adjustable in the range 18−47 nm by controlling the diameter of CNTs in the range 4−20 nm. The thicknesses of the CNT layers as well as the performances of the CNT-based UF membranes are highly correlated with the sprayed volumes of CNT dispersions. The resultant CNT-based UF membranes exhibit superior separation performances compared with state-of-the-art membranes as well as commercial membranes with similar pore sizes. This work provides an efficient and facile solution for alleviating the dependence to organic solvents and mitigating the environmental threat in the preparation of UF membranes. Moreover, by using different water-dispersible low-dimensional building blocks, for instance, nanoparticles, nanofibers, and nanosheets, this spraying-based process is expected to prepare other types of membranes in a solvent-free, clean manner.

■ ASSOCIATED CONTENT

Supporting Information

The Supporting Information is available free of charge at https://pubs.acs.org/doi/10.1021/acsestwater.2c00125.

Figures of FTIR characterization of CNT membrane, SEM images and water contact angles of CNT membranes, abrasion resistance, and long-term stability of CNT-1 membrane and table of performance comparison with membranes reported in the literature

https://doi.org/10.1021/acsestwater.2c00125
ACS EST Water 2022, 2, 895−903

and with commercial membranes with similar pore sizes (PDF)

AUTHOR INFORMATION

Corresponding Author

Yong Wang − *State Key Laboratory of Materials-Oriented Chemical Engineering, College of Chemical Engineering, Nanjing Tech University, Nanjing 211816 Jiangsu, P. R. China;* orcid.org/0000-0002-8653-514X; Email: yongwang@njtech.edu.cn; Fax: 0086-25-8317 2292

Authors

Dongwei Ma − *State Key Laboratory of Materials-Oriented Chemical Engineering, College of Chemical Engineering, Nanjing Tech University, Nanjing 211816 Jiangsu, P. R. China*

Xiangyue Ye − *State Key Laboratory of Materials-Oriented Chemical Engineering, College of Chemical Engineering, Nanjing Tech University, Nanjing 211816 Jiangsu, P. R. China*

Xiansong Shi − *State Key Laboratory of Materials-Oriented Chemical Engineering, College of Chemical Engineering, Nanjing Tech University, Nanjing 211816 Jiangsu, P. R. China;* orcid.org/0000-0002-4258-7941

Jiemei Zhou − *State Key Laboratory of Materials-Oriented Chemical Engineering, College of Chemical Engineering, Nanjing Tech University, Nanjing 211816 Jiangsu, P. R. China*

Complete contact information is available at: https://pubs.acs.org/10.1021/acsestwater.2c00125

Notes

The authors declare no competing financial interest.

ACKNOWLEDGMENTS

This work was supported by the National Science Fund for Distinguished Young Scholars (21825803).

REFERENCES

(1) Hampu, N.; Werber, J. R.; Chan, W. Y.; Feinberg, E. C.; Hillmyer, M. A. Next-Generation Ultrafiltration Membranes Enabled by Block Polymers. *ACS Nano* **2020**, *14*, 16446−16471.

(2) Guillen, G. R.; Pan, Y.; Li, M.; Hoek, E. M. V. Preparation and Characterization of Membranes Formed by Nonsolvent Induced Phase Separation: A Review. *Ind. Eng. Chem. Res.* **2011**, *50*, 3798−3817.

(3) Nunes, S. P.; Culfaz-Emecen, P. Z.; Ramon, G. Z.; Visser, T.; Koops, G. H.; Jin, W.; Ulbricht, M. Thinking the Future of Membranes: Perspectives for Advanced and New Membrane Materials and Manufacturing Processes. *J. Membr. Sci.* **2020**, *598*, 117761.

(4) Coria, J. Policy Monitor—the Economics of Toxic Substance Control and the Reach Directive. *Rev. Envir. Econ. Policy* **2018**, *12*, 342−358.

(5) Razali, M.; Kim, J. F.; Attfield, M.; Budd, P. M.; Drioli, E.; Lee, Y. M.; Szekely, G. Sustainable Wastewater Treatment and Recycling in Membrane Manufacturing. *Green Chem.* **2015**, *17*, 5196−5205.

(6) Xie, W.; Li, T.; Tiraferri, A.; Drioli, E.; Figoli, A.; Crittenden, J. C.; Liu, B. Toward the Next Generation of Sustainable Membranes from Green Chemistry Principles. *ACS Sustain. Chem. Eng.* **2021**, *9*, 50−75.

(7) Zou, D.; Nunes, S. P.; Vankelecom, I. F. J.; Figoli, A.; Lee, Y. M. Recent Advances in Polymer Membranes Employing Non-Toxic Solvents and Materials. *Green Chem.* **2021**, *23*, 9815−9843.

(8) Figoli, A.; Marino, T.; Simone, S.; Di Nicolò, E.; Li, X. M.; He, T.; Tornaghi, S.; Drioli, E. Towards Non-Toxic Solvents for Membrane Preparation: A Review. *Green Chem.* **2014**, *16*, 4034−4059.

(9) Dong, X.; Jeong, T. J.; Kline, E.; Banks, L.; Grulke, E.; Harris, T.; Escobar, I. C. Eco-Friendly Solvents and Their Mixture for the Fabrication of Polysulfone Ultrafiltration Membranes: An Investigation of Doctor Blade and Slot Die Casting Methods. *J. Membr. Sci.* **2020**, *614*, 118510.

(10) Wang, B.; Ji, J.; Li, K. Crystal Nuclei Templated Nanostructured Membranes Prepared by Solvent Crystallization and Polymer Migration. *Nat. Commun.* **2016**, *7*, 12804.

(11) Shah, V.; Wang, B.; Li, K. Blending Modification to Porous Polyvinylidene Fluoride (PVDF) Membranes Prepared via Combined Crystallisation and Diffusion (CCD) Technique. *J. Membr. Sci.* **2021**, *618*, 118708.

(12) Jin, W.; Toutianoush, A.; Tieke, B. Use of Polyelectrolyte Layer-by-Layer Assemblies as Nanofiltration and Reverse Osmosis Membranes. *Langmuir* **2003**, *19*, 2550−2553.

(13) Reurink, D. M.; Haven, J. P.; Achterhuis, I.; Lindhoud, S.; Roesink, H. D. W.; de Vos, W. M. Annealing of Polyelectrolyte Multilayers for Control over Ion Permeation. *Adv. Mater. Interfaces* **2018**, *5*, 1800651.

(14) Sadman, K.; Delgado, D. E.; Won, Y.; Wang, Q.; Gray, K. A.; Shull, K. R. Versatile and High-Throughput Polyelectrolyte Complex Membranes via Phase Inversion. *ACS Appl. Mater. Interfaces* **2019**, *11*, 16018−16026.

(15) Baig, M. I.; Durmaz, E. N.; Willott, J. D.; de Vos, W. M. Sustainable Membrane Production through Polyelectrolyte Complexation Induced Aqueous Phase Separation. *Adv. Funct. Mater.* **2020**, *30*, 1907344.

(16) Liang, H. W.; Wang, L.; Chen, P. Y.; Lin, H. T.; Chen, L. F.; He, D.; Yu, S. H. Carbonaceous Nanofiber Membranes for Selective Filtration and Separation of Nanoparticles. *Adv. Mater.* **2010**, *22*, 4691−4695.

(17) Liang, H.-W.; Cao, X.; Zhang, W.-J.; Lin, H.-T.; Zhou, F.; Chen, L.-F.; Yu, S.-H. Robust and Highly Efficient Free-Standing Carbonaceous Nanofiber Membranes for Water Purification. *Adv. Funct. Mater.* **2011**, *21*, 3851−3858.

(18) Brady-Estévez, A. S.; Kang, S.; Elimelech, M. A Single-Walled-Carbon-Nanotube Filter for Removal of Viral and Bacterial Pathogens. *Small* **2008**, *4*, 481−484.

(19) Srivastava, A.; Srivastava, O. N.; Talapatra, S.; Vajtai, R.; Ajayan, P. M. Carbon Nanotube Filters. *Nat. Mater.* **2004**, *3*, 610−614.

(20) Ma, D.; Li, H.; Meng, Z.; Zhang, C.; Zhou, J.; Xia, J.; Wang, Y. Absolute and Fast Removal of Viruses and Bacteria from Water by Spraying-Assembled Carbon-Nanotube Membranes. *Environ. Sci. Technol.* **2021**, *55*, 15206−15214.

(21) Shi, Z.; Zhang, W.; Zhang, F.; Liu, X.; Wang, D.; Jin, J.; Jiang, L. Ultrafast Separation of Emulsified Oil/Water Mixtures by Ultrathin Free-Standing Single-Walled Carbon Nanotube Network Films. *Adv. Mater.* **2013**, *25*, 2422−2427.

(22) Zhu, Y.; Xie, W.; Gao, S.; Zhang, F.; Zhang, W.; Liu, Z.; Jin, J. Single-Walled Carbon Nanotube Film Supported Nanofiltration Membrane with a Nearly 10 Nm Thick Polyamide Selective Layer for High-Flux and High-Rejection Desalination. *Small* **2016**, *12*, 5034−5041.

(23) Wang, Z.; Wang, Z.; Lin, S.; Jin, H.; Gao, S.; Zhu, Y.; Jin, J. Nanoparticle-Templated Nanofiltration Membranes for Ultrahigh Performance Desalination. *Nat. Commun.* **2018**, *9*, 2004−2012.

(24) Gao, S.; Zhu, Y.; Gong, Y.; Wang, Z.; Fang, W.; Jin, J. Ultrathin Polyamide Nanofiltration Membrane Fabricated on Brush-Painted Single-Walled Carbon Nanotube Network Support for Ion Sieving. *ACS Nano* **2019**, *13*, 5278−5290.

(25) Zhou, Z. Y.; Hu, Y. X.; Boo, C.; Liu, Z. Y.; Li, J. Q.; Deng, L. Y.; An, X. C. High-Performance Thin-Film Composite Membrane with an Ultrathin Spray-Coated Carbon Nanotube Interlayer. *Environ. Sci. Technol. Lett.* **2018**, *5*, 243−248.
(26) Ma, D.; Zhou, J.; Wang, Z.; Wang, Y. Block Copolymer Ultrafiltration Membranes by Spray Coating Coupled with Selective Swelling. *J. Membr. Sci.* **2020**, *598*, 117656.
(27) Zhao, L.; Chang, P. C. Y.; Yen, C.; Ho, W. S. W. High-Flux and Fouling-Resistant Membranes for Brackish Water Desalination. *J. Membr. Sci.* **2013**, *425−426*, 1−10.
(28) Chen, X.; Qiu, M.; Ding, H.; Fu, K.; Fan, Y. A Reduced Graphene Oxide Nanofiltration Membrane Intercalated by Well-Dispersed Carbon Nanotubes for Drinking Water Purification. *Nanoscale* **2016**, *8*, 5696−5705.
(29) Liu, Y.; Gao, G.; Vecitis, C. D. Prospects of an Electroactive Carbon Nanotube Membrane toward Environmental Applications. *Acc. Chem. Res.* **2020**, *53*, 2892−2902.

https://doi.org/10.1021/acsestwater.2c00125
ACS EST Water 2022, 2, 895−903